Piezo2 integrates mechanical and thermal cues in vertebrate mechanoreceptors

Wang Zheng[a,1], Yury A. Nikolaev[a,1], Elena O. Gracheva[a,b,c,2], and Sviatoslav N. Bagriantsev[a,2]

[a]Department of Cellular and Molecular Physiology, Yale University School of Medicine, New Haven, CT 06520; [b]Department of Neuroscience, Yale University School of Medicine, New Haven, CT 06520; and [c]Program in Cellular Neuroscience, Neurodegeneration and Repair, Yale University School of Medicine, New Haven, CT 06520

Edited by Joseph S. Takahashi, University of Texas Southwestern Medical Center, Dallas, TX, and approved July 23, 2019 (received for review June 13, 2019)

Tactile information is detected by thermoreceptors and mechanoreceptors in the skin and integrated by the central nervous system to produce the perception of somatosensation. Here we investigate the mechanism by which thermal and mechanical stimuli begin to interact and report that it is achieved by the mechanotransduction apparatus in cutaneous mechanoreceptors. We show that moderate cold potentiates the conversion of mechanical force into excitatory current in all types of mechanoreceptors from mice and tactile-specialist birds. This effect is observed at the level of mechanosensitive Piezo2 channels and can be replicated in heterologous systems using Piezo2 orthologs from different species. The cold sensitivity of Piezo2 is dependent on its blade domains, which render the channel resistant to cold-induced perturbations of the physical properties of the plasma membrane and give rise to a different mechanism of mechanical activation than that of Piezo1. Our data reveal that Piezo2 is an evolutionarily conserved mediator of thermal–tactile integration in cutaneous mechanoreceptors.

Piezo2 | Piezo1 | mechanoreceptor | cold receptor | polymodal ion channel

The mechanically gated ion channel Piezo2 mediates the detection of touch by somatosensory neurons and Merkel cells. Defects in Piezo2 function lead to severe deficits in mechanosensation, proprioception, and joint development in mice and humans (1–10). As a membrane protein in cutaneous mechanoreceptors, Piezo2 encounters thermal fluctuations in its environment, which in warm-blooded animals are often colder than the temperature of the body. Observations in humans have shown that prolonged cold exposure leads to numbness, likely due to inhibition of the action potential-generating machinery, whereas mild temporary cooling sharpens tactile acuity and enhances the perception of object heaviness by mechanosensitive Aβ fibers (11–14). Many vertebrates, including tactile-foraging waterfowl, are able to use the sense of touch to find food in cold water, demonstrating preservation of tactile acuity upon temporary cooling (15–17). These observations suggest that thermal and mechanical cues interact at the level of peripheral mechanoreceptors, and further, that cold may directly potentiate the conversion of mechanical force into excitatory current via Piezo2.

Piezo1, the only known homolog of Piezo2, mediates the detection of mechanical force in various cell types inside the body, including interoceptive mechanoreceptors from the nodose ganglion and neurons in the central nervous system (CNS), where it does not encounter significant fluctuations in temperature (18–20). Piezo1 activation is thought to be triggered primarily by membrane tension (21–26). Such reliance on "force-from-lipid" for activation suggests that cold would inhibit Piezo1 due to a decrease in membrane fluidity and increase in bending stiffness. Conversely, Piezo2 is refractory to activation by membrane stretch (8, 27–29), suggesting that Piezo2 may be resistant to cold-induced perturbations of the physical properties of the plasma membrane due to a different mechanism of activation.

The goal of this study was to investigate whether thermal and mechanical stimuli are integrated at the level of peripheral mechanoreceptors. We found that cold increases the peak amplitude of mechanically activated (MA) current in all mechanoreceptor subtypes from mice. Additionally, cold prolongs the time of MA current inactivation, leading to an overall potentiation of the amount of current entering the neuron upon mechanical stimulation. The effect is evolutionarily conserved, as similar cold-induced potentiation was also observed in mechanoreceptors from tactile-specialist birds. Cold also enhanced MA current through Piezo2 following its expression in various cell types, revealing the molecular basis for cold-induced potentiation of mechanosensitivity in a subset of mechanoreceptors. In contrast, cold inhibited MA current through Piezo1, supporting the idea that this homolog is acutely sensitive to changes in the physical properties of the plasma membrane. Similarly, stiffening the membrane with saturated fatty acids also inhibited Piezo1 but consistently failed to affect Piezo2. Swapping the membrane-embedded blade domains between Piezo2 and Piezo1 transposed the response of the 2 channels to cold or fatty acids, and thus their sensitivity to membrane stiffness. Together, these results reveal that somatosensory neurons can directly integrate thermal and mechanical stimuli via Piezo2, and that such integration is dependent on the blade domains of the channel.

Results

Cooling Potentiates MA Current in Mechanoreceptors from Different Species. Given the observation that mild temporary cooling sharpens tactile acuity (11–13), we sought to determine the effects

Significance

The detection of mechanical touch and temperature is essential for interaction with the physical world. Here, we report that cold potentiates the conversion of mechanical touch into excitatory ionic current in cutaneous mechanoreceptors from different vertebrate species. We show that this process is mediated by the mechanically gated ion channel Piezo2, the principal detector of touch in somatosensory neurons, and can be recapitulated by Piezo2 orthologs in various heterologous systems. We demonstrate that the blade domains are essential for cold-induced potentiation of Piezo2 activity and are sufficient to endow this property when transposed onto Piezo2 homolog Piezo1. Our findings provide mechanistic insights into thermal–tactile interaction in vertebrates at the level of somatosensory neurons.

Author contributions: W.Z., Y.A.N., E.O.G., and S.N.B. designed research; W.Z., Y.A.N., and E.O.G. performed research; W.Z., Y.A.N., E.O.G., and S.N.B. analyzed data; and W.Z., Y.A.N., E.O.G., and S.N.B. wrote the paper.

The authors declare no conflict of interest.

This article is a PNAS Direct Submission.

Data deposition: The squirrel Piezo2 reported in this paper has been deposited in the GenBank database (accession no. MK905889).

[1]W.Z. and Y.A.N. contributed equally to this work.

[2]To whom correspondence may be addressed. Email: elena.gracheva@yale.edu or sviatoslav.bagriantsev@yale.edu.

This article contains supporting information online at www.pnas.org/lookup/suppl/doi:10.1073/pnas.1910213116/-/DCSupplemental.

Published online August 14, 2019.

of cold on mechanotransduction in somatosensory neurons. We recorded MA current in mouse dorsal root ganglion (DRG) neurons in response to mechanical indentation with a glass probe at 22 °C, a standard temperature for MA current recordings (30), followed by 12 °C, a temperature that engages the majority of cold receptors (31). We found that cooling from 22 °C to 12 °C enhanced the amount of current flowing through MA channels by slowing inactivation and increasing peak current amplitude. We observed this effect in each of the 3 major groups of somatosensory neurons: those with fast, intermediate, and slowly inactivating MA current (Fig. 1 *A–D* and *SI Appendix*, Fig. S1*A*). Together, the 3 groups encompass low-threshold mechanoreceptors, high-threshold mechanonociceptors, and proprioceptors (32).

We next asked whether cold-induced potentiation is evolutionarily conserved and whether it is present in mechanoreceptors from the trigeminal ganglion (TG), a cranial analog of the DRG that provides sensory innervation to the face in vertebrates. To do this, we analyzed neurons from the TG of Pekin duck (*Anas platyrhynchos domesticus*), a tactile-specialist bird (15). The largest neuronal group in duck TG are Piezo2-expressing low-threshold mechanoreceptors, which support the specialized tactile feeding apparatus in the bill (33–35). Like other vertebrates, the duck TG lacks proprioceptors. Similar to mouse DRG neurons, cooling from 22 °C to 12 °C slowed inactivation and increased the peak amplitude of MA current in each of the 3 groups of duck trigeminal mechanoreceptors (Fig. 1 *E–H*). Cooling failed to elicit MA current in mechanically insensitive neurons from either species (*SI Appendix*, Fig. S1 *B* and *C*). Collectively, these data show that cooling increases the amount of excitatory current in mechanoreceptors during mechanical stimulation. Further, because this integration of thermal and mechanical cues was observed in all types of mechanoreceptors from mammals and birds, the data demonstrate evolutionary conservation of the underlying molecular mechanisms.

Cooling Potentiates Piezo2-Mediated MA Current. The mechanically gated ion channel Piezo2 mediates fast inactivating MA current in low-threshold mechanoreceptors and proprioceptors from mouse DRG (1, 4, 36). To investigate whether Piezo2 channels mediate the effects of cold-induced potentiation of mechanical responses, we tested the effect of cold on Piezo2 expressed in ND7/23 cells, a DRG neuron-derived cell line with low levels of endogenous MA current (37) (*SI Appendix*, Fig. S2*A*). We found that cooling from 22 °C to 12 °C slowed the inactivation kinetics of MA current through Piezo2 and increased peak amplitude at negative membrane potentials, resulting in a dramatic increase in the total charge conducted by Piezo2 in response to mechanical stimulation. The effect was fully reversible upon rewarming to 22 °C (Fig. 2 *A* and *B* and *SI Appendix*, Fig. S2 *B* and *C*). We also observed a reversible cold-induced potentiation of mouse Piezo2 MA current in *Piezo1*-deficient neuroblastoma-derived N2A ($N2A^{\Delta P1}$) and HEK293T ($HEK293T^{\Delta P1}$) cells at positive and negative potentials (Fig. 2 *C* and *D* and *SI Appendix*, Fig. S2 *D–G*) (27, 38, 39). Furthermore, cold temperatures slowed MA current inactivation in $HEK293T^{\Delta P1}$ cells expressing Piezo2 orthologs cloned from Pekin duck, a tactile-specialist bird, and 13-lined ground squirrel (*Ictidomys tridecemlineatus*), a rodent that exhibits a remarkable cold tolerance at the level of the somatosensory system (Fig. 2 *E–H* and *SI Appendix*, Fig. S2 *H–K*) (40). The similarity of these data to those from DRG and TG neurons suggests that cold-induced potentiation of fast MA current in somatosensory neurons is mediated by Piezo2 channels.

To obtain a more detailed picture of the effect of cooling on Piezo2, we recorded MA current in $HEK293T^{\Delta P1}$ cells expressing mouse Piezo2 at a broad range of temperatures from 37 °C to 9 °C. We found that Piezo2 inactivation has a sigmoid dependence on temperature, reaching a near-maximum at ∼12 °C and a near-minimum at ∼22 °C, whereas peak current amplitude is temperature-independent (Fig. 2 *I* and *J*). Thus, the increase in Piezo2 MA current amplitude upon cooling requires the native environment of somatosensory neurons or the related ND7/23 cell line. It is possible that the neurons and ND7/23 cell express additional mechanotransducers or components of the mechanotransduction machinery, which may account for the potentiating effect of cold on MA current amplitude compared to HEK293 cells. Nevertheless, because slowing of current inactivation is independent of cell type, we can conclude that cold enhances the total amount of MA current flowing through Piezo2 channels from birds to mammals.

Cooling Inhibits Piezo1-Mediated MA Current. To examine whether the effect of cold on MA currents is specific to Piezo2, we tested its close homolog Piezo1, which is expressed in vagal sensory neurons, CNS neurons, and various other cell types in the body (18–20). We found that cooling from 22 °C to 12 °C slowed inactivation of mechanical indentation-evoked Piezo1 current in $HEK293T^{\Delta P1}$ cells at negative and positive potentials. However, in stark contrast to Piezo2, cold significantly suppressed Piezo1 peak current amplitude (Fig. 3 *A* and *B* and *SI Appendix*, Fig. S3). We observed a similar diminution of MA current amplitude when we stimulated Piezo1 by stretching the plasma membrane with a high-speed pressure clamp in the cell-attached configuration (Fig. 3 *C* and *D*). For both methods, inhibition was reversible upon rewarming to 22 °C. Sampling Piezo1 activity at a range of temperatures from 37 °C to 9 °C revealed that cooling slows inactivation and inhibits peak amplitude with a sigmoid dependence such that both parameters reach saturation at 12 °C (Fig. 3 *E* and *F*). Single-channel recordings of spontaneous Piezo1 activity under the basal tension of a cell-attached patch (41) showed that cooling from 22 °C to 12 °C decreases open probability and reduces single-channel conductance, whereas warming from 22 °C to 32 °C or 37 °C increases only conductance (Fig. 3 *G–J*). Thus, our data demonstrate that, in contrast to the potentiating effect on Piezo2, cooling inhibits mechanically evoked activity of Piezo1.

Membrane Stiffness Inhibits MA Currents through Piezo1 but Not Piezo2. Cooling exerts multiple effects on the cell, including an increase in structural order of plasma membrane lipids. As a result, a cooled membrane has decreased fluidity and increased bending stiffness (42). Qualitatively similar changes in the plasma membrane can be achieved at room temperature by incubating the cells with margaric acid (MarA), a C17 saturated fatty acid (43). To examine whether membrane stiffness underlies the differential effects of cooling on Piezo1 and Piezo2, we tested the mechanosensitivity of Piezo1 and Piezo2 expressed in $HEK293T^{\Delta P1}$ cells preincubated with 50 μM MarA. Consistent with an earlier report using N2A cells (43), we found that MarA inhibited the peak amplitude of MA current through Piezo1 without affecting inactivation (Fig. 4 *A–C*). Single-channel analysis revealed that inhibition stemmed from a decrease in Piezo1 open probability (Fig. 4 *D* and *E*). In agreement with the effect of cooling, MarA failed to diminish MA current produced by Piezo2 (Fig. 4 *F–H*). These results demonstrate that, unlike Piezo1, mechanical activation of Piezo2 is insensitive to changes in membrane stiffness, providing an explanation for the lack of an inhibitory effect of cold on peak amplitude of Piezo2 MA current.

The Blade Domains Determine Sensitivity to Cold and Membrane Stiffness. Structural studies have revealed that Piezo1 is composed of 3 monomers, each containing a blade domain on the N terminus and a pore-forming C-terminal domain (44–46). The blade domains are integrated into the plasma membrane such that they produce a cup-shaped structure with the pore in the center. The curved blades are thought to serve as essential channel elements that detect an increase in membrane tension to

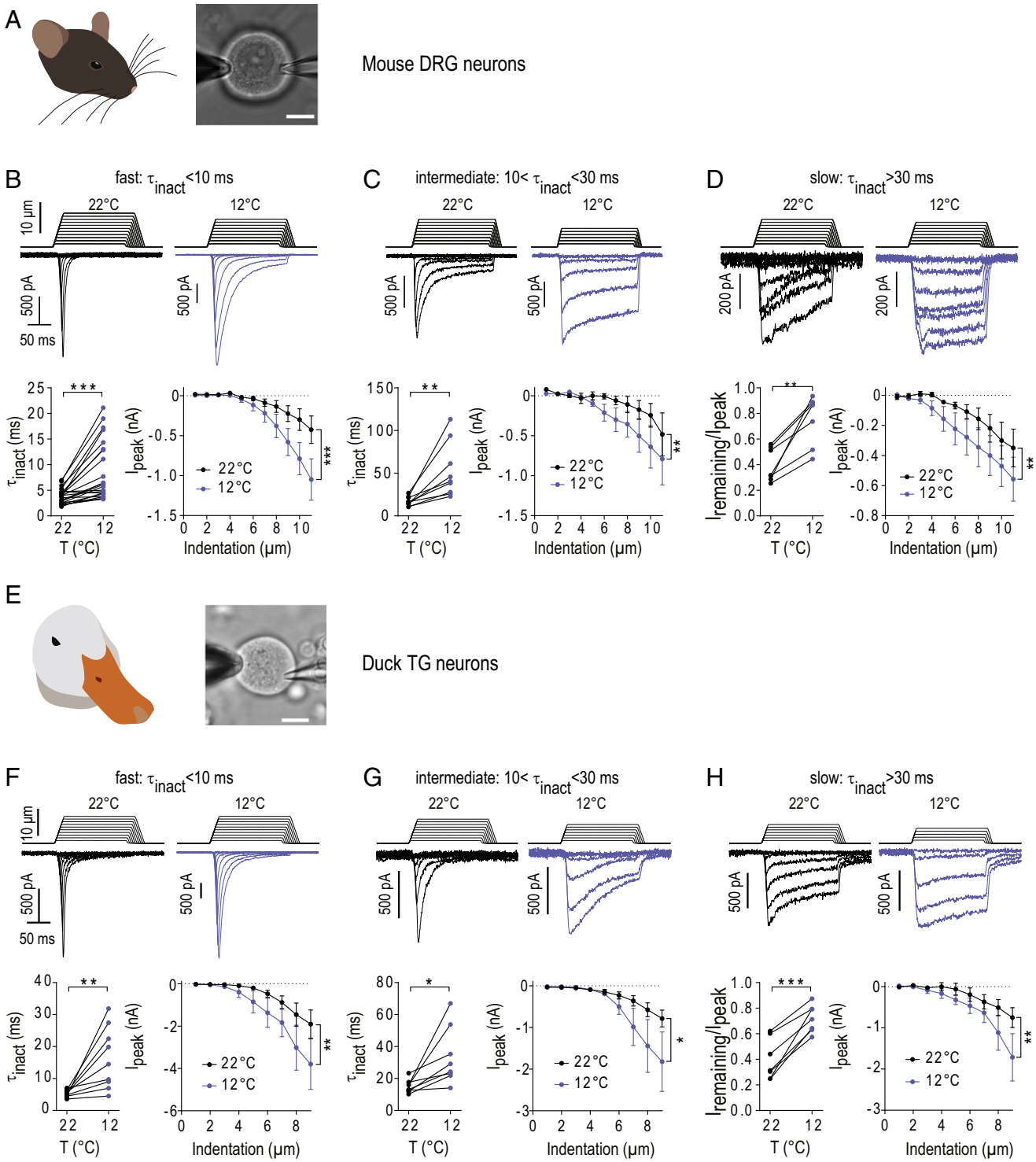

Fig. 1. Cooling potentiates mechanotransduction in somatosensory neurons from mouse DRG and duck TG. (*A* and *E*) Images of neurons dissociated from mouse DRG (*A*) and duck TG (*E*), with the recording pipette and the glass probe (*Right* and *Left*, respectively) in the working positions. (Scale bars, 10 μm.) (*B–D* and *F–H*) (*Upper*) Representative whole-cell MA current traces recorded in mechanoreceptors from mouse DRG (*B–D*) or duck TG (*F–H*) at 22 °C or 12 °C in response to mechanical indentation of the soma to the indicated depth. E_{hold} = –60 mV. MA currents are classified based on inactivation rate (τ_{inact}) at 22 °C. (*Lower*) Quantification of the effect of cooling on MA current inactivation and peak amplitude. Inactivation was quantified by fitting the decaying component of MA current to the exponential equation (τ_{inact}) for neurons with fast and intermediate MA current, or by measuring the fraction of remaining MA current at the end of stimulation ($I_{remaining}/I_{peak}$) for neurons with slow MA current. **P* < 0.05, ***P* < 0.01, ****P* < 0.001, paired *t* test or 2-way ANOVA. For I_{peak} plots, data are mean ± SEM from 5 to 13 cells.

cause opening of the pore via the "force-from-lipid" mechanism (26, 47, 48). We therefore hypothesized that the differential effects of cold and MarA on Piezo1 and Piezo2 are a result of the different blade domains. To test our hypothesis, we measured MA currents at 12 °C, 22 °C, and 37 °C in HEK293T$^{\Delta P1}$ cells expressing Piezo1/2 chimeras in which the blade domains were

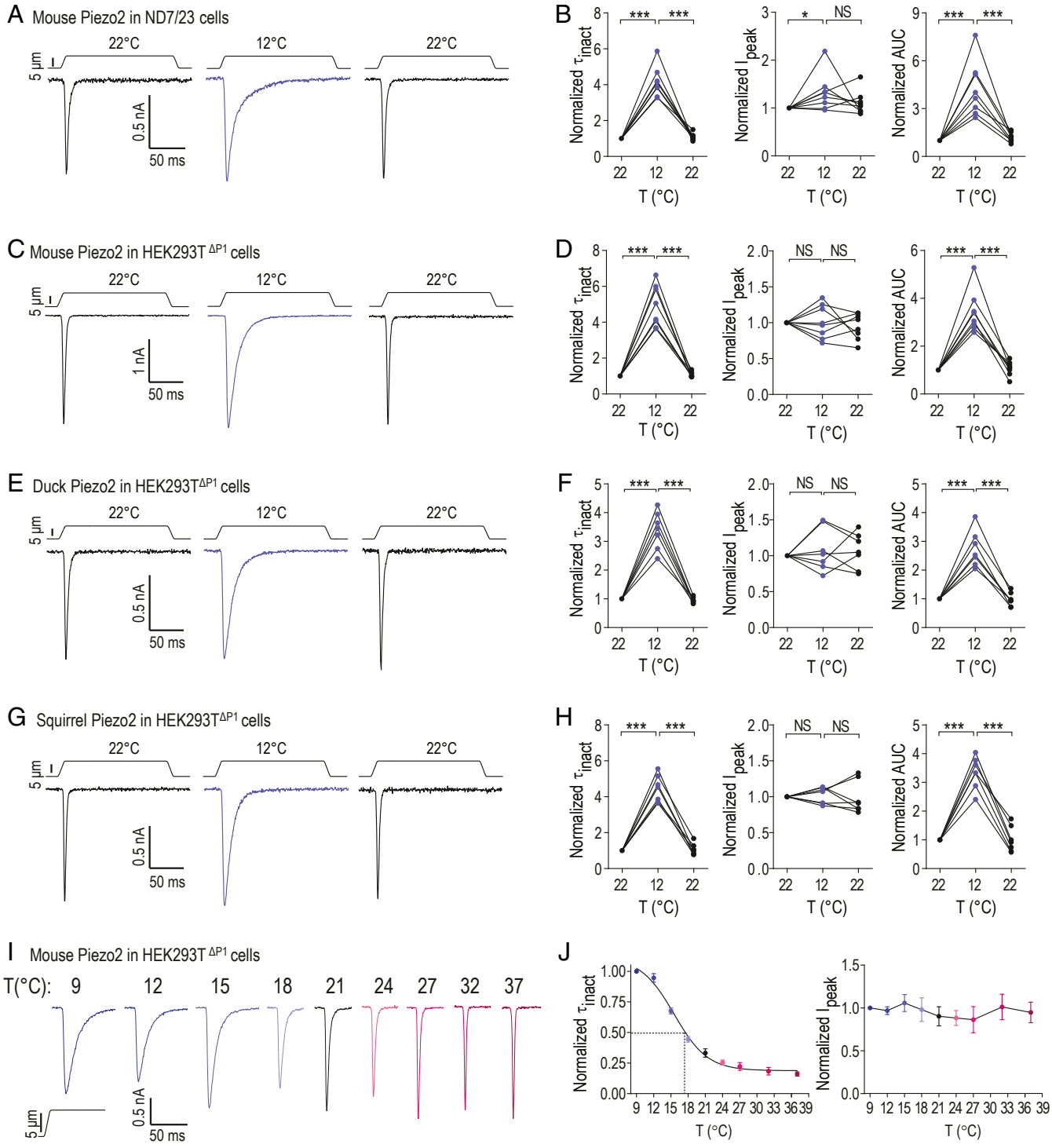

Fig. 2. Cooling potentiates Piezo2-mediated MA current. (*A*, *C*, *E*, and *G*) Representative whole-cell MA current traces consecutively recorded at indicated temperatures from mouse Piezo2 in ND7/23 (*A*), mouse Piezo2 in HEK293T$^{\Delta P1}$ (*C*), duck Piezo2 in HEK293T$^{\Delta P1}$ (*E*), and squirrel Piezo2 in HEK293T$^{\Delta P1}$ (*G*). E_{hold} = −80 mV. (*B*, *D*, *F*, and *H*) Quantification of the effect of temperature on MA current parameters recorded at −80 mV and normalized to initial values at 22 °C: MA current inactivation (τ_{inact}, *Left*), peak MA current amplitude (I_{peak}, *Middle*) and total amount of conducted charge estimated as area under the current curve (AUC, *Right*) recorded from mouse Piezo2 in ND7/23 (*B*), mouse Piezo2 (*D*), duck Piezo2 (*F*), or squirrel Piezo2 (*H*) in HEK293T$^{\Delta P1}$. (*I*) Representative whole-cell MA current traces recorded from mouse Piezo2 in the same HEK293T$^{\Delta P1}$ cell at indicated temperatures during cooling from 37 °C to 9 °C. E_{hold} = −80 mV. (*J*) Quantification of the effect of cooling on mouse Piezo2 MA current τ_{inact} (*Left*) and I_{peak} (*Right*) in HEK293T$^{\Delta P1}$. Data are mean ± SEM from 7 cells. NS, not significant, $P > 0.05$, *$P < 0.05$, ***$P < 0.001$, paired *t* test.

swapped (27). We found that a chimera containing Piezo1 blades fused to the Piezo2 pore (P1^{blade}/P2^{pore}; Fig. 5*A*) responds to cooling and MarA like wild-type Piezo1. Cooling from 37 °C to 12 °C slowed P1^{blade}/P2^{pore} inactivation and significantly inhibited current amplitude (Fig. 5 *B* and *C*). Pretreatment with MarA inhibited MA peak current amplitude in this chimera but did not

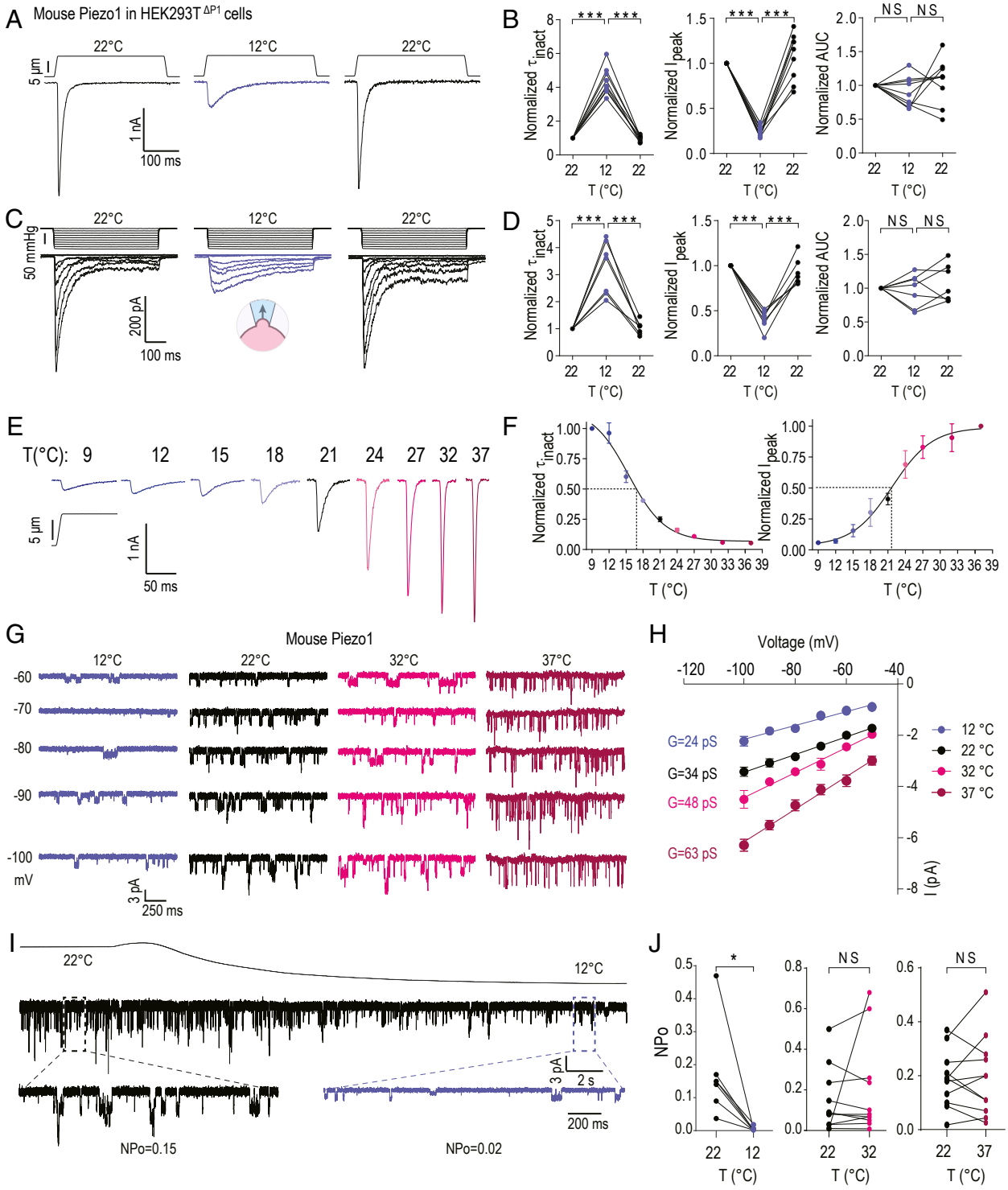

Fig. 3. Cooling inhibits Piezo1-mediated MA current. (*A*) Representative whole-cell MA current traces recorded at indicated temperatures in the same HEK293T$^{\Delta P1}$ cell expressing mouse Piezo1. E_{hold} = −80 mV. MA currents were elicited with the same indentation depth. (*B*) Normalized MA current τ_{inact} (*Left*), I_{peak} (*Middle*), and area under the current curve (AUC, *Right*) from *A*. NS, not significant, $P > 0.05$; ***$P < 0.001$, paired *t* test. (*C*) Representative cell-attached MA current traces at indicated temperatures in the same HEK293T$^{\Delta P1}$ cell expressing mouse Piezo1. E_{hold} = −80 mV. Currents are induced by negative pressures applied by high-speed pressure clamp in the recording electrode, as shown. (*D*) Normalized τ_{inact}, I_{peak}, or AUC of maximum MA current from (*C*). NS, not significant, $P > 0.05$; ***$P < 0.001$, paired *t* test. (*E* and *F*) Representative whole-cell MA current traces at temperatures ranging from 9 °C to 37 °C in the same HEK293T$^{\Delta P1}$ cell expressing mouse Piezo1 (*E*) and quantification of normalized MA current τ_{inact} and I_{peak} (*F*) (n = 7 cells). E_{hold} = −80 mV. (*G*) Representative single-channel recordings of mouse Piezo1 in HEK293T$^{\Delta P1}$ cells in cell-attached mode. Spontaneous Piezo1 openings were recorded at basal membrane tension in the cell-attached patch without application of additional pressure, at indicated temperatures and voltages. Downward deflections represent inward current. (*H*) Current-voltage relationships for single Piezo1 channel at indicated temperatures from (*G*) with single channel conductances: 12 °C, 24.8 ± 2.1 pS; 22 °C, 34.6 ± 1.3 pS; 32 °C, 48.7 ± 2.6 pS, 37 °C, 63.75 ± 3.4 pS (mean ± SEM, n = 5 cells for each temperature). (*I*) Representative mouse Piezo1 single-channel recording at −100 mV from the HEK293T$^{\Delta P1}$ cell with temperature cooled from 22 °C to 12 °C. Enlarged sections of the current trace are shown at 22 °C and 12 °C with corresponding open probabilities (NPo). (*J*) Quantification of the temperature effect on NPo of Piezo1 by cooling (*Left*) and warming (*Right*). NS, not significant, $P > 0.05$; *$P < 0.05$, paired *t* test. Data are mean ± SEM.

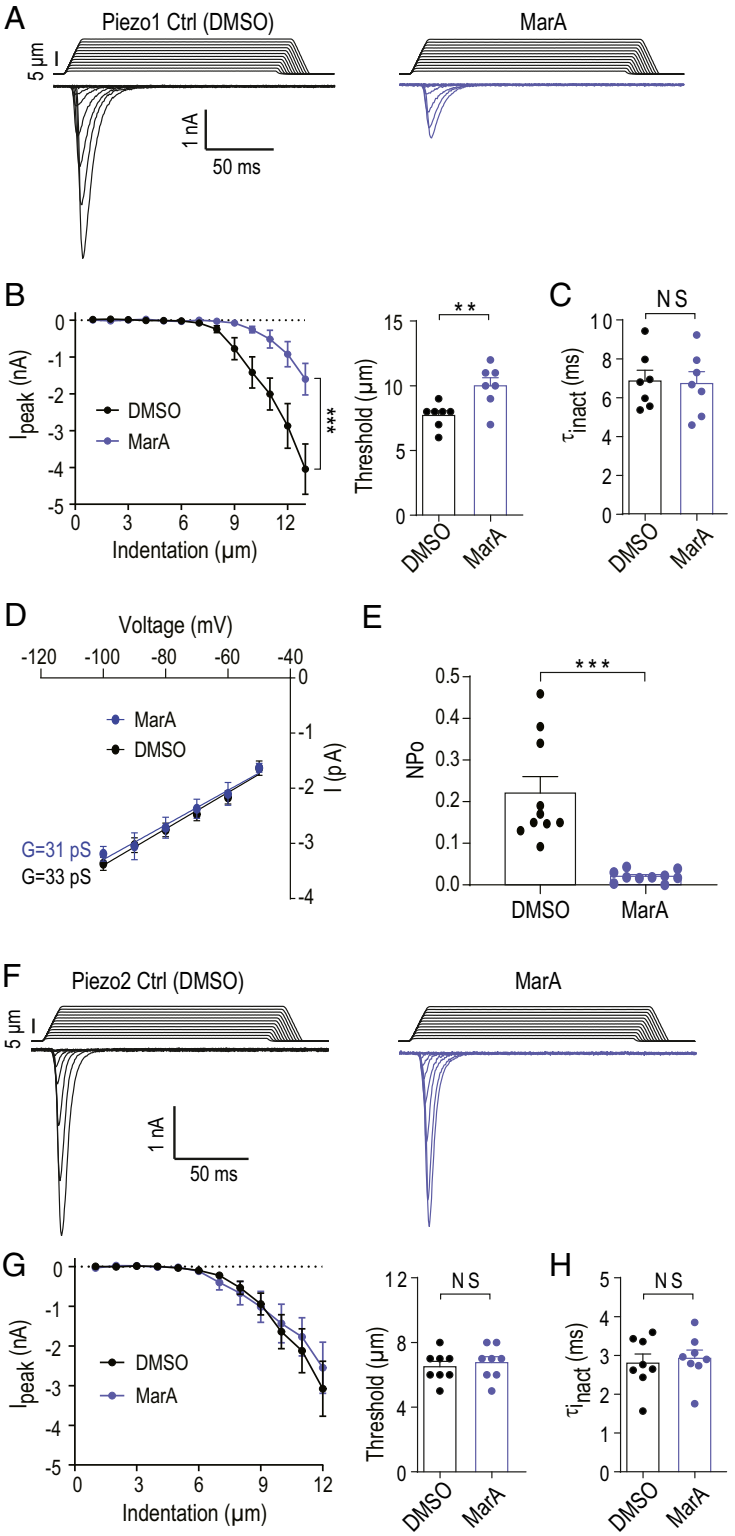

Fig. 4. Stiffening the plasma membrane inhibits mechanical activation of Piezo1 but not Piezo2. (*A*) Representative whole-cell MA current traces recorded at room temperature in HEK293T$^{\Delta P1}$ cells expressing mouse Piezo1. E_{hold} = −80 mV. Cells were treated with 50 µM margaric acid (MarA) or the same volume of DMSO for 18 to 24 h before current measurements. (*B*) Quantification of MA current I_{peak} and apparent activation threshold from *A* (n = 7 cells). (*C*) Quantification of MA current τ_{inact} from *A*. NS, not significant, $P > 0.05$, unpaired t test. (*D*) Current-voltage relationships of single Piezo1 channel from HEK293T$^{\Delta P1}$ cells treated with 50 µM MarA (n = 3 cells) or the same volume of DMSO (n = 3 cells). Estimated single-channel conductances: DMSO, 33.0 ± 2.7 pS; MarA, 31.4 ± 3.8 pS. (*E*) Quantification of Piezo1 open probability (NPo) at −80 mV from HEK293T$^{\Delta P1}$ cells treated with 50 µM MarA or DMSO (n = 10 cells). (*F*) Representative whole-cell MA current traces at room temperature in HEK293T$^{\Delta P1}$ cells expressing mouse Piezo2. E_{hold} = −80 mV. Cells were treated with 50 µM MarA or DMSO. (*G*) Quantification of MA current I_{peak} and threshold from (*F*) (n = 8 cells). (*H*) Quantification of MA current τ_{inact} from (*F*). Data are mean ± SEM. NS, not significant, $P > 0.05$, $^{**}P < 0.01$, $^{***}P < 0.001$, unpaired t test or 2-way ANOVA.

affect inactivation (Fig. 5 *D* and *E*). Conversely, a chimera composed of Piezo2 blades and Piezo1 pore ($P2^{blade}/P1^{pore}$; Fig. 5*F*) behaved similarly to Piezo2. Cooling from 37 °C to 12 °C slowed inactivation of MA current through $P2^{blade}/P1^{pore}$, without affecting peak current amplitude, leading to an increase in the total charge conducted (Fig. 5 *G* and *H*). Similar to cold application, pretreatment with MarA failed to inhibit the peak amplitude of $P2^{blade}/P1^{pore}$ currents and even slightly increased it (Fig. 5 *I* and *J*). Thus, the sensitivity to changes in membrane stiffness induced by cooling or MarA is encoded by the blade domains of Piezo1 and Piezo2. These observations suggest that, in contrast to Piezo1, "force-from-lipid" may not be the major pathway of Piezo2 activation, but the exact mechanism remains to be determined.

Discussion

The integration of sensory modalities occurs within the CNS and results in cognitive awareness of our surroundings (49–52). The work reported here shows that, in addition to this central integration, thermal and mechanical stimuli begin to interact at the level of cutaneous mechanoreceptors. This conclusion is based on our observation that cooling increases the peak and sustained amplitude of MA current in somatosensory neurons from mouse DRG, leading to a large increase in the amount of depolarizing charge that enters the neuron in response to mechanical stimulation. Interestingly, cold potentiated MA current magnitude in all types of mouse mechanoreceptors, including those with fast, intermediate, and slow MA current. In rodents, fast MA current

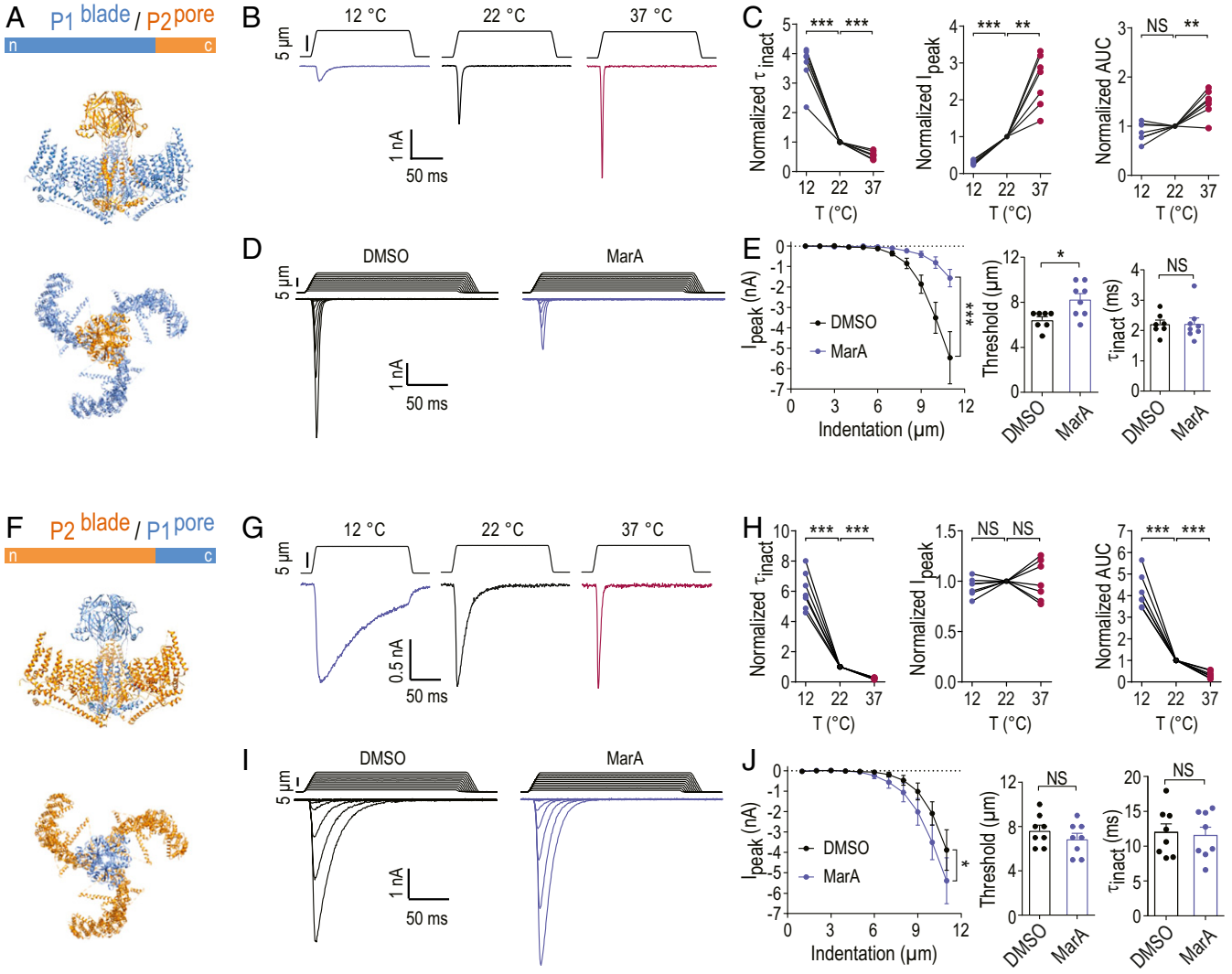

Fig. 5. Blade domains mediate sensitivity of Piezo channels to cold. (*A*) Illustrations of $P1^{blade}/P2^{pore}$ chimera construct containing mouse Piezo1 blade domains (blue) and mouse Piezo2 pore domains (orange). (*B* and *C*) Representative whole-cell MA current traces in the same $HEK293T^{\Delta P1}$ cell expressing the $P1^{blade}/P2^{pore}$ chimera construct (*B*) and normalized MA current τ_{inact}, I_{peak}, and area under the current curve, AUC (*C*). E_{hold} = −80 mV. NS, not significant, $P > 0.05$; $^{**}P < 0.01$, $^{***}P < 0.001$, paired *t* test. (*D* and *E*) Representative whole-cell MA current traces recorded at room temperature in $HEK293T^{\Delta P1}$ cells expressing $P1^{blade}/P2^{pore}$ (*D*) and quantification of MA current I_{peak}, apparent activation threshold or τ_{inact}. E_{hold} = −80 mV. Cells were treated with 50 µM MarA (n = 8 cells) or DMSO (n = 7 cells) for 18 to 24 h before current measurements. NS, not significant, $^{*}P < 0.05$, $^{***}P < 0.001$, 2-way ANOVA or unpaired *t* test. (*F*) Illustrations of $P2^{blade}/P1^{pore}$ chimera construct containing mouse Piezo2 blade domains (orange) and mouse Piezo1 pore domains (blue). (*G* and *H*) Representative whole-cell MA current traces in the same $HEK293T^{\Delta P1}$ cell expressing the $P2^{blade}/P1^{pore}$ chimera construct (*G*) and quantification of normalized MA current, τ_{inact}, I_{peak}, and AUC (*H*). E_{hold} = −80 mV. NS, not significant, $P > 0.05$; $^{***}P < 0.001$, paired *t* test. (*I* and *J*) Representative whole-cell MA current traces recorded at room temperature in $HEK293T^{\Delta P1}$ cells expressing $P2^{blade}/P1^{pore}$ (*I*) and quantification of MA current I_{peak}, apparent activation threshold or τ_{inact} (*J*). E_{hold} = −80 mV. Cells were treated with 50 µM MarA (n = 8 cells) or DMSO (n = 8 cells). NS, not significant, $P > 0.05$; $^{*}P < 0.05$, 2-way ANOVA or unpaired *t* test. Data are mean ± SEM.

is present in light touch receptors and proprioceptors, whereas intermediate and slow MA currents are mostly thought to define mechanical nociceptors (32).

We also detected a similar potentiation of mechanical responses in somatosensory neurons from the TG of tactile-foraging ducks. Like all vertebrates, the TG of tactile-foraging ducks is devoid of proprioceptors. However, in contrast to other vertebrates, including rodents and visually foraging birds, duck TG contains an unusually high proportion of light touch receptors that develop at the expense of nociceptors and thermoreceptors. This results in mechanosensory specialization in the bill toward tactile foraging (33–35). The commonality between the potentiating effects of cold on MA current in mouse and duck somatosensory ganglia strongly suggests that the peripheral integration of thermal and mechanical cues is an evolutionarily conserved property of vertebrate mechanoreceptors.

Fast MA current in mouse DRG neurons is mediated by Piezo2, whereas the molecular identity of intermediate and slow MA channels remains obscure (4, 36). We show that ectopic expression of mouse, squirrel, or duck Piezo2 orthologs in various heterologous systems recapitulates the potentiating effect of cold on fast MA current in neurons, providing a molecular basis for the observed effect in this mechanoreceptor subtype.

With the exception of physiological cold sensors, such as TRPM8 and some orthologs of TRPA1, a decrease in temperature generally inhibits ion channels, including those that generate action potentials (14, 53–56). We suggest that the preservation of Piezo2 function during cold stimuli may serve as a mechanism to support the functionality of mechanoreceptors upon cooling. This property would be important for the ability of warm-blooded animals to physically interact with objects that are often colder than the body, or for duck species to find food in cold water during their tactile-based dabbling behavior (15, 17). In humans, although prolonged cold exposure leads to numbness, mild temporary cooling potentiates mechanosensitivity. Indeed, a cold object is perceived as heavier than the same object at a neutral temperature. Cooling also potentiates tactile acuity in 2-point discrimination tests on various parts of the body. Such a thermotactile illusion, known as Weber's phenomenon, is attenuated upon partial blockade of Aβ fibers, suggesting a direct involvement of mechanoreceptors (11–13). Correspondingly, cooling induces a phasic discharge of slowly adapting Aβ mechanoreceptors in mammals and birds (16, 57, 58). In mice, the fast inactivating MA current in these slowly adapting mechanoreceptors is mediated by Piezo2 (4). In agreement with these findings, we have shown that cold enhances MA current through Piezo2 channels in neurons and cell lines, which explains at least some of the observed integration of thermal and tactile stimuli in mechanoreceptors.

Despite their significance for physiology and medicine, the mechanism by which Piezo channels activate in response to mechanical stimulation remains obscure. Piezo1 forms a unique propeller-like structure with a pore in the center and 3 curved blades that bestow a cup-like shape on the channel (44–46). The curved shape of the channel results in a convex membrane footprint, which is thought to be the source of energy for channel gating in response to changes in membrane stiffness and tension (26). Experimental evidence supports the idea that Piezo1 is primarily activated by membrane tension via the "force-from-lipid" mechanism (21–25, 48). Piezo2, on the other hand, is refractory to activation by membrane stretch, supporting the idea that it may activate via other mechanisms, such as "force-from-tether" (27–29, 59, 60). We have shown that stiffening the plasma membrane with cold temperatures or saturated fatty acids inhibits activation of Piezo1 but fails to affect Piezo2, and that this difference is encoded by the blade domains. Thus, our data provide strong evidence for the notion that Piezo1 and Piezo2 activate by different mechanisms, despite sequence homology and functional similarities between the 2 channels. Specifically, in contrast to Piezo1, activation of Piezo2 does not appear to be directly linked to changes in physical properties of the plasma membrane. Our observations also predict that the unidentified mechanotransducers that mediate intermediate and slow MA current in mouse DRG should be activated via a mechanism similar to Piezo2.

Following activation, MA current produced by Piezo1 or Piezo2 quickly decays due to fast inactivation (61). Mutations that affect inactivation in either channel are linked to disease, and thus the timing of this process has physiological importance (9, 62–64). Inactivation is influenced by cellular factors and is thought to involve a hydrophobic gate formed primarily by the inner helices plus other regions including the extracellular cap (23, 61, 65–68). Whether inactivation is governed by changes in plasma membrane properties is unclear. We show that inactivation is slowed by cooling, but not membrane stiffening, in both Piezo1 and Piezo2. These observations raise the possibility that inactivation stems from conformational changes within the channels and is generally independent of the physical properties of the plasma membrane.

In conclusion, we have shown that cold potentiates MA current in all types of mechanoreceptors from different vertebrates. At least some of this effect is due to the potentiation of current flowing through mechanosensitive Piezo2 channels, whereas the rest is mediated by unidentified mechanotransducers, whose activity is also expected to be potentiated by cold. We show that cold sensitivity of Piezo2 is conveyed by its blade domains. The underlying mechanism is independent of the physical properties of the plasma membrane, revealing that Piezo2 is activated by a different mechanism to that of Piezo1. Together, our data reveal that Piezo2 mediates thermal–tactile integration in cutaneous mechanoreceptors from evolutionary divergent species.

Materials and Methods

Experiments with mice, squirrels, and Pekin duck embryos were approved by and performed in accordance with guidelines of Institutional Animal Case and Use Committee of Yale University (protocols 2018-11526 and 2018-11497). HEK293T$^{\Delta P1}$, N2A$^{\Delta P1}$ (27, 38) and ND7/23 cells were cultured using standard procedures. Duck-Piezo2-pMO and Mouse-Piezo1-pMO were described previously (67). Squirrel Piezo2 was amplified from squirrel DRG cDNA and deposited into the GenBank database (accession no. MK905889). DRG neurons from 6- to 8-wk-old mice and TG neurons from embryonic day 22 to 24 duck embryos were acutely dissociated as previously described (34, 35). Electrophysiological recordings of MA currents from neurons and cell lines were performed at different temperatures in the whole-cell mode in response to indentation with a glass probe (35, 67, 69). For cell-attached experiments, mechanical stimuli were applied by negative pressure pulses using a high-speed pressure clamp system (70). For a detailed description, see *SI Appendix, Supplementary Methods*.

ACKNOWLEDGMENTS. We thank members of the S.N.B. and E.O.G. laboratories for their contributions throughout the project and Evan Anderson for comments on the manuscript. W.Z. was supported by fellowships from James Hudson Brown - Alexander B. Coxe and the Kavli Institute for Neuroscience. This study was partly funded by NIH grants 1R01NS091300-01A1 (to E.O.G.) and 1R01NS097547-01A1 (to S.N.B.), by NSF CAREER award 1453167 (to S.N.B.), and NSF grant 1923127 (to S.N.B.).

1. E. O. Anderson, E. R. Schneider, S. N. Bagriantsev, Piezo2 in cutaneous and proprioceptive mechanotransduction in vertebrates. *Curr. Top. Membr.* **79**, 197–217 (2017).
2. A. T. Chesler *et al*., The role of PIEZO2 in human mechanosensation. *N. Engl. J. Med.* **375**, 1355–1364 (2016).
3. M. Szczot *et al*., PIEZO2 mediates injury-induced tactile pain in mice and humans. *Sci. Transl. Med.* **10**, eaat9892 (2018).
4. S. S. Ranade *et al*., Piezo2 is the major transducer of mechanical forces for touch sensation in mice. *Nature* **516**, 121–125 (2014).
5. S. E. Murthy *et al*., The mechanosensitive ion channel Piezo2 mediates sensitivity to mechanical pain in mice. *Sci. Transl. Med.* **10**, eaat9897 (2018).
6. S. Maksimovic *et al*., Epidermal Merkel cells are mechanosensory cells that tune mammalian touch receptors. *Nature* **509**, 617–621 (2014).

7. S. H. Woo *et al*., Piezo2 is required for Merkel-cell mechanotransduction. *Nature* **509**, 622–626 (2014).
8. R. Ikeda *et al*., Merkel cells transduce and encode tactile stimuli to drive Aβ-afferent impulses. *Cell* **157**, 664–675 (2014).
9. B. Coste *et al*., Gain-of-function mutations in the mechanically activated ion channel PIEZO2 cause a subtype of distal arthrogryposis. *Proc. Natl. Acad. Sci. U.S.A.* **110**, 4667–4672 (2013).
10. B. Coste *et al*., Piezo1 and Piezo2 are essential components of distinct mechanically activated cation channels. *Science* **330**, 55–60 (2010).
11. J. C. Stevens, Temperature can sharpen tactile acuity. *Percept. Psychophys.* **31**, 577–580 (1982).
12. J. S. Dunn, D. A. Mahns, S. S. Nagi, Why does a cooled object feel heavier? Psychophysical investigations into the Weber's phenomenon. *BMC Neurosci.* **18**, 4 (2017).
13. J. C. Stevens, B. G. Green, Temperature-touch interaction: Weber's phenomenon revisited. *Sens. Processes* **2**, 206–209 (1978).
14. K. Zimmermann *et al*., Sensory neuron sodium channel Nav1.8 is essential for pain at low temperatures. *Nature* **447**, 855–858 (2007).
15. E. R. Schneider, E. O. Gracheva, S. N. Bagriantsev, Evolutionary specialization of tactile perception in vertebrates. *Physiology (Bethesda)* **31**, 193–200 (2016).
16. K. M. Gottschaldt, H. Fruhstorfer, W. Schmidt, I. Kräft, Thermosensitivity and its possible fine-structural basis in mechanoreceptors in the beak skin of geese. *J. Comp. Neurol.* **205**, 219–245 (1982).
17. G. A. Zweers, *Mechanics of the Feeding of the Mallard (Anas Platyrhynchos, L.; Aves, Anseriformes)* (S. Karger AG, ed. 1, 1977).
18. D. E. Koser *et al*., Mechanosensing is critical for axon growth in the developing brain. *Nat. Neurosci.* **19**, 1592–1598 (2016).
19. Y. Song *et al*., The mechanosensitive ion channel Piezo inhibits axon regeneration. *Neuron* **102**, 373–389.e6 (2019).
20. W. Z. Zeng *et al*., PIEZOs mediate neuronal sensing of blood pressure and the baroreceptor reflex. *Science* **362**, 464–467 (2018).
21. A. H. Lewis, J. Grandl, Mechanical sensitivity of Piezo1 ion channels can be tuned by cellular membrane tension. *eLife* **4**, e12088 (2015).
22. J. Wu, R. Goyal, J. Grandl, Localized force application reveals mechanically sensitive domains of Piezo1. *Nat. Commun.* **7**, 12939 (2016).
23. J. Wu *et al*., Inactivation of mechanically activated Piezo1 ion channels is determined by the C-terminal extracellular domain and the inner pore helix. *Cell Rep.* **21**, 2357–2366 (2017).
24. C. D. Cox *et al*., Removal of the mechanoprotective influence of the cytoskeleton reveals PIEZO1 is gated by bilayer tension. *Nat. Commun.* **7**, 10366 (2016).
25. R. Syeda *et al*., Piezo1 channels are inherently mechanosensitive. *Cell Rep.* **17**, 1739–1746 (2016).
26. C. A. Haselwandter, R. MacKinnon, Piezo's membrane footprint and its contribution to mechanosensitivity. *eLife* **7**, e41968 (2018).
27. M. Moroni, M. R. Servin-Vences, R. Fleischer, O. Sánchez-Carranza, G. R. Lewin, Voltage gating of mechanosensitive PIEZO channels. *Nat. Commun.* **9**, 1096 (2018).
28. J. Hu, L. Y. Chiang, M. Koch, G. R. Lewin, Evidence for a protein tether involved in somatic touch. *EMBO J.* **29**, 855–867 (2010).
29. W. Zhang *et al*., Ankyrin repeats convey force to gate the NOMPC mechanotransduction channel. *Cell* **162**, 1391–1403 (2015).
30. J. Hao, P. Delmas, Recording of mechanosensitive currents using piezoelectrically driven mechanostimulator. *Nat. Protoc.* **6**, 979–990 (2011).
31. D. D. McKemy, The molecular and cellular basis of cold sensation. *ACS Chem. Neurosci.* **4**, 238–247 (2013).
32. P. Delmas, J. Hao, L. Rodat-Despoix, Molecular mechanisms of mechanotransduction in mammalian sensory neurons. *Nat. Rev. Neurosci.* **12**, 139–153 (2011).
33. E. R. Schneider *et al*., A cross-species analysis reveals a general role for Piezo2 in mechanosensory specialization of trigeminal ganglia from tactile specialist birds. *Cell rep.* **26**, 1979–1987.e3 (2019).
34. E. R. Schneider *et al*., Molecular basis of tactile specialization in the duck bill. *Proc. Natl. Acad. Sci. U.S.A.* **114**, 13036–13041 (2017).
35. E. R. Schneider *et al*., Neuronal mechanism for acute mechanosensitivity in tactile-foraging waterfowl. *Proc. Natl. Acad. Sci. U.S.A.* **111**, 14941–14946 (2014).
36. S. H. Woo *et al*., Piezo2 is the principal mechanotransduction channel for proprioception. *Nat. Neurosci.* **18**, 1756–1762 (2015).
37. J. N. Wood *et al*., Novel cell lines display properties of nociceptive sensory neurons. *Proc. Biol. Sci.* **241**, 187–194 (1990).
38. A. E. Dubin *et al*., Endogenous Piezo1 can confound mechanically activated channel identification and characterization. *Neuron* **94**, 266–270.e3 (2017).
39. V. Lukacs *et al*., Impaired PIEZO1 function in patients with a novel autosomal recessive congenital lymphatic dysplasia. *Nat. Commun.* **6**, 8329 (2015).
40. V. Matos-Cruz *et al*., Molecular prerequisites for diminished cold sensitivity in ground squirrels and hamsters. *Cell Rep.* **21**, 3329–3337 (2017).
41. T. M. Suchyna, V. S. Markin, F. Sachs, Biophysics and structure of the patch and the gigaseal. *Biophys. J.* **97**, 738–747 (2009).
42. J. Pan, S. Tristram-Nagle, N. Kucerka, J. F. Nagle, Temperature dependence of structure, bending rigidity, and bilayer interactions of dioleoylphosphatidylcholine bilayers. *Biophys. J.* **94**, 117–124 (2008).
43. L. O. Romero *et al*., Dietary fatty acids fine-tune Piezo1 mechanical response. *Nat. Commun.* **10**, 1200 (2019).
44. Y. R. Guo, R. MacKinnon, Structure-based membrane dome mechanism for Piezo mechanosensitivity. *eLife* **6**, e33660 (2017).
45. K. Saotome *et al*., Structure of the mechanically activated ion channel Piezo1. *Nature* **554**, 481–486 (2018)
46. Q. Zhao *et al*., Structure and mechanogating mechanism of the Piezo1 channel. *Nature* **554**, 487–492 (2018).
47. Y. Wang *et al*., A lever-like transduction pathway for long-distance chemical- and mechano-gating of the mechanosensitive Piezo1 channel. *Nat. Commun.* **9**, 1300 (2018).
48. C. D. Cox, N. Bavi, B. Martinac, Origin of the force: The force-from-lipids principle applied to Piezo channels. *Curr. Top. Membr.* **79**, 59–96 (2017).
49. A. Barik, J. H. Thompson, M. Seltzer, N. Ghitani, A. T. Chesler, A brainstem-spinal circuit controlling nocifensive behavior. *Neuron* **100**, 1491–1503.e3 (2018).
50. J. Braz, C. Solorzano, X. Wang, A. I. Basbaum, Transmitting pain and itch messages: A contemporary view of the spinal cord circuits that generate gate control. *Neuron* **82**, 522–536 (2014).
51. J. Huang *et al*., Circuit dissection of the role of somatostatin in itch and pain. *Nat. Neurosci.* **21**, 707–716 (2018).
52. A. L. Zimmerman *et al*., Distinct modes of presynaptic inhibition of cutaneous afferents and their functions in behavior. *Neuron* **102**, 420–434.e8 (2019).
53. S. Jabba *et al*., Directionality of temperature activation in mouse TRPA1 ion channel can be inverted by single-point mutations in ankyrin repeat six. *Neuron* **82**, 1017–1031 (2014).
54. D. D. McKemy, W. M. Neuhausser, D. Julius, Identification of a cold receptor reveals a general role for TRP channels in thermosensation. *Nature* **416**, 52–58 (2002).
55. L. Moparthi *et al*., Human TRPA1 is intrinsically cold- and chemosensitive with and without its N-terminal ankyrin repeat domain. *Proc. Natl. Acad. Sci. U S A* **111**, 16901–16906 (2014).
56. W. J. Laursen, E. O. Anderson, L. J. Hoffstaetter, S. N. Bagriantsev, E. O. Gracheva, Species-specific temperature sensitivity of TRPA1. *Temperature (Austin)* **2**, 214–226 (2015).
57. R. Duclaux, D. R. Kenshalo, The temperature sensitivity of the type I slowly adapting mechanoreceptors in cats and monkeys. *J. Physiol.* **224**, 647–664 (1972).
58. H. Burton, S. I. Terashima, J. Clark, Response properties of slowly adapting mechanoreceptors to temperature stimulation in cats. *Brain Res.* **45**, 401–416 (1972).
59. R. Ikeda, J. G. Gu, Piezo2 channel conductance and localization domains in Merkel cells of rat whisker hair follicles. *Neurosci. Lett.* **583**, 210–215 (2014).
60. S. Katta, M. Krieg, M. B. Goodman, Feeling force: Physical and physiological principles enabling sensory mechanotransduction. *Annu. Rev. Cell Dev. Biol.* **31**, 347–371 (2015).
61. P. A. Gottlieb, C. Bae, F. Sachs, Gating the mechanical channel Piezo1: A comparison between whole-cell and patch recording. *Channels (Austin)* **6**, 282–289 (2012).
62. C. Bae, R. Gnanasambandam, C. Nicolai, F. Sachs, P. A. Gottlieb, Xerocytosis is caused by mutations that alter the kinetics of the mechanosensitive channel PIEZO1. *Proc. Natl. Acad. Sci. U.S.A.* **110**, E1162–E1168 (2013).
63. J. Albuisson *et al*., Dehydrated hereditary stomatocytosis linked to gain-of-function mutations in mechanically activated PIEZO1 ion channels. *Nat. Commun.* **4**, 1884 (2013).
64. E. Glogowska *et al*., Novel mechanisms of PIEZO1 dysfunction in hereditary xerocytosis. *Blood* **130**, 1845–1856 (2017).
65. W. Zheng, E. O. Gracheva, S. N. Bagriantsev, A hydrophobic gate in the inner pore helix is the major determinant of inactivation in mechanosensitive Piezo channels. *eLife* **8**, e44003 (2019).
66. B. Coste *et al*., Piezo1 ion channel pore properties are dictated by C-terminal region. *Nat. Commun.* **6**, 7223 (2015).
67. E. O. Anderson, E. R. Schneider, J. D. Matson, E. O. Gracheva, S. N. Bagriantsev, TMEM150C/Tentonin3 is a regulator of mechano-gated ion channels. *Cell Rep.* **23**, 701–708 (2018).
68. F. J. Taberner *et al*., Structure-guided examination of the mechanogating mechanism of PIEZO2. *Proc. Natl. Acad. Sci. U.S.A.* **116**, 14260–14269 (2019).
69. J. Hao *et al*., Piezo-electrically driven mechanical stimulation of sensory neurons. *Methods Mol. Biol.* **998**, 159–170 (2013).
70. S. R. Besch, T. Suchyna, F. Sachs, High-speed pressure clamp. *Pflugers Arch.* **445**, 161–166 (2002).

PNAS
www.pnas.org

Supplementary Information for

Piezo2 integrates mechanical and thermal cues in vertebrate mechanoreceptors

Wang Zheng, Yury A. Nikolaev, Elena O. Gracheva, and Sviatoslav N. Bagriantsev

Sviatoslav N. Bagriantsev
Email: slav.bagriantsev@yale.edu

This PDF file includes:

Supplementary Methods
Figures S1 to S3
Supplementary References

www.pnas.org/cgi/doi/10.1073/pnas.1910213116

Supplementary Methods

Animals. Experiments with mice and Pekin duck embryos (*Anas platyrhynchos domesticus*) were approved by and performed in accordance with guidelines of Institutional Animal Case and Use Committee of Yale University (protocols 2018-11526 and 2018-11497). C57BL/6J mice were purchased from The Jackson Laboratory and maintained in Yale animal facilities. Fertilized duck eggs were purchased from Metzer Farms (Gonzales, CA) and incubated at 37ºC as described previously (1).

cDNA constructs. The Mouse-Piezo2-Sport6 construct was kindly provided Ardem Patapoutian (Scripps Research Institute, CA) (2). Duck-Piezo2-pMO and Mouse-Piezo1-pMO were described previously (3). Squirrel-Piezo2-pcDNA3.1(+) was constructed as described below. Chimera constructs $P1^{blade}/P2^{pore}$, containing blade domains from mouse Piezo1 and pore domains from mouse Piezo2 (Piezo1 amino acids 1-2190; Piezo2 amino acids 2472-2822), and $P2^{blade}/P1^{pore}$, containing blade domains from mouse Piezo2 and pore domains from mouse Piezo1 (Piezo2 amino acids 1-2471; Piezo1 amino acids 2188-2547), were kind gifts from Gary Lewin (Max Delbrück Center for Molecular Medicine, Germany) (4).

Cell culture and transfection. HEK293T and N2A cells with genomic deletion of *PIEZO1* ($HEK293T^{\Delta P1}$ and $N2A^{\Delta P1}$) were provided by Ardem Patapoutian (Scripps Research Institute) (5) and Gary Lewin (Max Delbrück Center for Molecular Medicine) (4). ND7/23 cells were purchased from Sigma-Aldrich (Cat# 92090903, St. Louis, MO). Cells were cultured in Dulbecco's modified Eagle's medium (DMEM) supplemented with 10% fetal bovine serum (FBS) and 1% penicillin/streptomycin (ThermoFisher Scientific, Waltham, MA). 1 mM sodium pyruvate was included in the medium for $N2A^{\Delta P1}$ and 2 mM L-glutamine was added for ND7/23 cells. Transient

transfection was performed using Lipofectamine 3000 (ThermoFisher, Waltham, MA) for Piezo1 or Lipofectamine 2000 (ThermoFisher) for Piezo2 according to the manufacturer's instructions.

Squirrel Piezo2 cloning. Squirrel Piezo2 (MK905889) was amplified from squirrel DRG cDNA using primers (forward 5'-3': GAGATGGCCTCGGAAGTGG; reverse 5'-3': AAGGTTCACATTACCCGCAG) and cloned into pcDNA3.1(+) vector. The cloned squirrel Piezo2 coding sequence was deposited into the GenBank database under the accession number MK905889 and the protein sequence was shown below:

MASEVVCGLVFRLLLPICLAVACAFRYNGLSFVYLIYLLLIPLFSEPTKATMQGHTGRLLKSLCFLSLSFLLLHIIF
HITLASLEAQHHITPGYNCSTWEKTFRQIGFESLKGADAGNGIRVFVPDIGMFIASLTIWLVCRNIVQKPVTEEAAQ
YNLEFENEELAAGEKADSEDALMDADADGDGAEGELEESAKLKMFRRVASVASKLKEFIGNMITTAGKVVVTVLLGS
SGMMLPSLTSAVYFFVFLGLCTWWSWCRTFDPLLFSCLCVLLAIFTAGHLIGLYLYQFQFFQEAVPPNDYYARLFGI
KSVIQTDCSSTWKIVVNPELSWYHHANPILLLVMYYTLATLIRIWLQEPLVQDEKTKEEDRSLVCSSNQRTAERKRN
LWYAAQYPTDERKLLSMTQDDYKPSDGLLVTVNGNPVDYHTIHPSLPLENGPAKTDLYSTPQYRWEPSEDSTEKKEE
EEDEKEEFEEERSQEEKRSVKVHAMVSVFQFIMKQSYICALIAMMAWSITYHSWLTFVLLIWSCALWMIRNRRKYAM
ISSPFMVVYANLLLVLQYIWSFELPEIKKVPGFLEKKEPGELASKILFTITFWLLLRQHLTEQKALQEKEALLSEVK
IGSQENEEKDEDLQDIQVEGEPKEKEEEEEAQEEEQEDEDEDQDIMKVLGNLVVAMFIKYWIYVCGGMFFFVSFEGK
IVMYKIIYMVLFLFCVALYQVHYEWWRKILKYFWMSVVIYTMLVLIFIYTYQFENFPGLWQNMTGLKKEKLEDLGLK
QFTVAELFTRIFIPTSFLLVCILHLHYFHDRFLELTDLKSIPRKEDNTIYSHAKVNGRVYLIINRLAHPEGSLPDLA
MMHLTASLERPEGKKLAELVDEKTEGSPGKAEKGELGEGSEEPEEGEDEEEESEEEEEMSDLRNKWHLVIDRLTVLF
LKSLEHFHKLQVFTWWILELHIIKIVSSYIIWVSVKEVSLFNYVFLISWAFALPYAKLRRVASSICTVWTCVIIVCK
MLYQLQTIKPESFSVNCSLPNENQTNIPLQDLNKSLLYSAPIDPTEWVGLRKSSPLLVYLRNNLLMLAILAFEVTIY
RHQEYYRGRNNLTAPVSKTIFHDITRMHLDDGLINCAKYFINYFFYKFGLETCFLMSVNVIGQRMDFYAMIHACWLI
AVLYRRRRKAIAEVWPKYCCFLACIITFQYFICIGIPPAPCRDYPWRFKGADFNDNIIKWLYFPDFIVRPNPVFLVY
DFMLLLCASLQRQIFEDENKAAVRIMAGDNVEICMNLDAASFSQHNPVPDFIHCRSYLDMSKVIIFSYLFWFVLTII
FITGTTRISIFCMGYLVACFYFLLFGGDLLLKPIKSILRYWDWLIAYNVFVITMKNILSIGACGYIGTLVKKSCWLI
QAFSLACTVKGYTMPEDDASCRLPSGEAGIIWDSICFAFLLLQRRVFMSYYFLHVVADIKASQILASRGAELFQATI
VKAVKARIEEEKRSMDQLKRQMDRIKARQQKYKKGKERMLSLTQEAGEGQDVQNPPEEDDEREADKQKAKGKKKQWW
RPWVDHASMVRSGDYYLFETDSEEEEEEELKKEDEGPPRKSAFQRAIGKFASAILALPKSVIKLPKTILQYLIRAAK
FVYQAWITDPKTALRQRRKEKKKSAREEQKRRRKGSGEGAVEWEDREDEPVKKKSDGPDNIIKRIFNILKFTWVLFL
ATVDSFTTWLNSISREHIDISTVLRIERCMLTREIKKGNVPTRESIHMYYQNHIMNLSRESGLDTLDERPGAAPGAQ
TAHRMDSLDSHDSISSCYTEATMLFSRQSTLDDLDGPDAVPKTSERARPRLRKMLSLDMSSSSADSGSLASSEPTQC
TMLYSRQGTTETIEEVEAEAEEEVVGPVPEPELELQPGDTQEEEEEEEEEAEYDLGPEEASLTPEEEECPQFSTDEG
DVEAPPSYSKAVSFEHLSFGSQDDSGGKNHMMVSPDDSRTDKLESSILPPLTHELTASELLLNKMFHDDELEESERF
YVGQPRFLLLFYAMYNTLVARSEMVCYFVIILNHMVSASMITLLLPILIFLWAMLSVPRPSRRFWMMAIVYTEVAIV
VKYFFQFGFFPWNKNVELYKDKPYHPPNIIGVEKKEGYVLYDLIQLLALFFHRSILKCHGLWDEDDIVDGGDQEESD
DEPSFSHGRRDSSDSLKSINLAASVESVHVTFPEQPTTIRRKRCGSSPQISPGSSFSSDRSKRGSTSTRNSSQKGSS
VLSIKQKSKRELYMEKLQEQLVKAKAFTIKKTLQIYVPIRQFFYDLIHPDYSAVTDVYVLMFLADTVDFIIIVFGFW
AFGKHSAAADITSSLSEDQVPGPFLVMVLIQFGTMVVDRALYLRKTVLGKVVFQVILVFGIHFWMFFILPVVTERKF
SQNLVAQLWYFVKCVYFGLSAYQIRCGYPTRVLGNFLTKSYNYVNLFLFQGFRLVPFLTELRAVMDWVWTDTTLSLS
SWICVEDIYAHIFILKCWRESEKRYPQPRGQKKKKVVKYGMGGMIIVLLICIVWFPLLFMSLIKSVAGVINQPLDVS
VTITLGGYQPIFTMSAQQSQLKVMDQTKFNKFMRTFSRDTGAMQFLENYEKEDITVAELEGNSNSLWTISPPSKQKM
ISELKDLSSSFSVVFSWSIQRNMSLGAKAEIATDKLSFPLQNSTRKNIANMIASNDPESSKTPVTIERIYPYYVKAP
SDSNSKPIKQLLSESNFMNITIILSRDNSTNSNSEWWVLNLTGNRIYDQESQALELVVFNDKVSPPSLGFLAGYGIM
GLYASVVLVIGKFVREFFSGISHSIMFEELPNVDRILKLCTDIFLVRETGELELEEDLYAKLIFLYRSPETMIKWTR
EKTN

Dissociation of mouse DRG neurons and duck TG neurons. DRG neurons from adult mouse (6-8 weeks old) and TG neurons from embryonic duck (E22-24) were acutely dissociated as previously described (1, 6). Specifically, dissected mouse DRG and duck TG were chopped briefly with scissors in 500 μl ice-cold HBSS and then dissociated by adding 500 μl 2 mg/ml collagenase (Roche, Basel, Switzerland, dissolved in HBSS) to a final concentration of 1 mg/ml, with incubation for 15 min at 37 °C. The collagenase solution was then removed and neurons at the bottom of the tube were incubated with 500 μl 0.25% trypsin-EDTA for 10 min at 37 °C. The trypsin was then removed and the residual trypsin was quenched by adding 750 μl pre-warmed DMEM+ medium (DMEM supplemented with 10% FBS, 1% penicillin/streptomycin and 2 mM glutamine). Cells were triturated gently with plastic P1000 and P200 pipette tips and then collected with centrifuge at 100 × g for 3 min. Next, cells were resuspended in DMEM+ medium and plated onto the Matrigel (BD Bioscience, Billerica, MA) -precoated coverslips in a 12-well cell-culture plate. 1 ml DMEM+ medium was added into each well following incubation at 37 °C in 5% CO_2 for 30-45 min. MA current measurements were then performed within 48 hours.

Patch-clamp electrophysiology. Whole-cell recordings of MA currents from heterologously expressed Piezo1 and Piezo2 were performed as described previously (3). The Piezo2 or Piezo1 constructs and pcDNA3-GFP plasmid were co-transfected into HEK293T$^{\Delta P1}$, N2A$^{\Delta P1}$ or ND7/23 cells in a 20:1 ratio. 24-48 hours after transfection, cells were plated onto matrigel (BD Bioscience) -coated coverslips and were recorded within 24 hours after plating. To test the effect of Margaric acid (MarA) (Sigma), cells were treated with 50 μM MarA or the same volume of DMSO when plating. The external solution contained (in mM): 140 NaCl, 5 KCl, 10 HEPES, 2.5 $CaCl_2$, 1 $MgCl_2$, 10 glucose (pH 7.4 adjusted with NaOH). The internal solution consisted of (in mM): 133 CsCl, 5 EGTA, 1 $CaCl_2$, 1 $MgCl_2$, 10 HEPES, 4 Mg-ATP, 0.4 Na_2-GTP

(pH 7.3 adjusted with CsOH). Recording pipettes of borosilicate glass with 1.5 mm outer diameter (Warner Instruments, Hamden, CT) were pulled to a tip resistance of 1-3 MΩ using a micropipette puller (Sutter Instruments, Novato, CA, model P-1000) and were polished with a polisher (ALA Scientific Instruments, Farmingdale, NY) before use. Series resistance and membrane capacitance were compensated at 85%. Currents were recorded using a Multi-clamp 700-B patch-clamp amplifier and Digidata 1500 digitizer (Molecular Devices, Union City, CA), sampled at 20kHz using a 500 MΩ feedback resistor and low-pass filtered at 10 kHz through an internal Bessel filter. Data were acquired and analyzed using the pClamp 10 software (Axon Instruments, Union City, CA). Mechanical stimulation were applied using a blunt glass probe (tip diameter, 2-4 μm) mounted on a pre-loaded Piezo actuator stack (Physik Instrumente, Karlsruhe, Germany) with the probe set to 30° from the horizontal plane (7). After break into the cell, the tip of the stimulation probe was positioned to just touch the cell membrane. The probe was then moved toward the cell at 1000 μm/s in 1-μm increments, held in position for 150 or 300 ms, retracted with the same speed. Cells were clamped at -80 mV during recordings, which were not corrected for liquid junction potential. The temperature of the external solution in the recording chamber was controlled by a bipolar temperature controller (Warner Instrument) and was constantly recorded with a thermal probe. Typically, the external solution was cooled from 22 °C to 12 °C or warmed up back to 22 °C within 30 s. The seal was maintained while changing the temperature. MA current recordings from dissociated mouse DRG or duck TG neurons were performed as previously described (1, 6) and were the same to those described above for cell lines, except that neurons were held at -60 mV (without liquid junction potential correction), the mechanical probe was advanced at 500 μm/s and recording pipettes were filled with internal solution containing (in mM): 130 K-methanesulfonate, 20 KCl, 1 $MgCl_2$, 10 HEPES, 3 Na_2ATP, 0.06 Na_3GTP, 0.2 EGTA, pH 7.3 (pH

adjusted with KOH, final [K^+] = 150.5 mM). To determine the MA current inactivation rate, the current decaying phase (between the peak point and the stimulus offset) was fitted to a single exponential function: $I = \Delta I * exp\hat{}(-t/\tau_{inact})$, where ΔI is the current amplitude from baseline to peak, t is the time span from the peak current to plateau, and τ_{inact} is the inactivation rate constant. The apparent MA current activation threshold was defined as the first indentation depth that elicit a peak current, typically at least 40 pA greater than background noise signal. The dependence of MA current amplitude and τ_{inact} on temperature were fitted to the sigmoid equations $Y=I_{min}+(I_{max}-I_{min})/(1+(T_{1/2}/T)\hat{}h)$ or $Y=\tau_{inact,min}+(\tau_{inact,max}-\tau_{inact,min})/(1+(T_{1/2}/T)\hat{}h)$, respectively, where $T_{1/2}$ is half-maximal effective temperature and h is the steepness of the curve.

Cell-attached recordings of Piezo1-elicited MA current in HEK293T$^{\Delta P1}$ cells were performed as described (3). Cells were prepared similarly to whole-cell recordings described above. The external solution contained (in mM): 140 KCl, 10 HEPES, 1 $MgCl_2$, 10 glucose, pH 7.3 (pH adjusted with KOH) and the internal solution was composed of (in mM): 130 NaCl, 5 KCl, 10 HEPES, 10 TEA-Cl, 1 $CaCl_2$, 1 $MgCl_2$, pH 7.3 (pH adjusted with NaOH). Recording patch pipettes of borosilicate glass were pulled and fire-polished to a tip resistance of 1-2 MΩ. Piezo1 stretch-activated current were acquired with pClamp 10 software and were recorded at a sampling frequency of 10 kHz with a 5 GΩ feedback resistor using a Multi-clamp 700-B patch-clamp amplifier and Digidata 1500 digitizer. Mechanical stimulations were performed by applying a family of 500 ms negative pressure pulses (Δ10 mmHg with 3 s between sweeps) using a high speed pressure clamp system (HSPC-1, ALA Scientific Instruments) (8). The membrane voltage inside the patch was clamped at -80 mV.

For single-channel recordings of Piezo1, HEK293T$^{\Delta P1}$ cells overexpressing Piezo1 were prepared as above. All single channel events were recorded in the cell-attached mode. While

applying a +10 mmHg pressure step (with HSPC) the pipette tip was immersed in the solution and after touching the cell the pressure was released until GΩ seal was formed. Bath solution contained (in mM): 140 KCl, 10 HEPES, 1 $MgCl_2$, 10 glucose, pH 7.3 (pH adjusted with KOH) and the pipette solution was composed of (in mM): 140 NaCl, 5 KCl, 10 HEPES, 1 EGTA, 1 $MgCl_2$, pH 7.4 (pH adjusted with NaOH). Single channel events are shown as down deflections at a given voltage (ΔV_{patch}) which represent inward current. Currents were sampled at 25 kHz and filtered at 1 kHz. For measuring Piezo1 NPo in MarA/DMSO treated cells: after pulling the glass pipette one of the paired electrodes was used in recordings with DMSO treatment and the other with MarA. The tip resistant range was 1-2 MΩ. Single channel data was analyzed using Clampfit 10.7. Mean single channel amplitudes were calculated by fitting the current-amplitude histograms with Gaussian curves at a given voltage. The unitary conductance values for Piezo1 single channel were obtained by fitting the slope to the current voltage relationship. Each NPo value was calculated from a 40 s period after applying 2 kHz Gaussian low-pass filter using Clampfit.

Quantification and statistical analysis. Data were analyzed and plotted using GraphPad Prism 7.01 (GraphPad Software Inc., La Jolla, CA) and expressed as means ± SEM. Statistical analyses were carried out using paired or unpaired t-tests when comparing two groups or two-way ANOVA for three or more groups, as specified in figure legends. Statistical tests were chosen based on sample size and normality of distribution. A probability value (P) of less than 0.05, 0.01, 0.001 was considered statistically significant and indicated by *, **, and ***, respectively.

Supplementary Figures

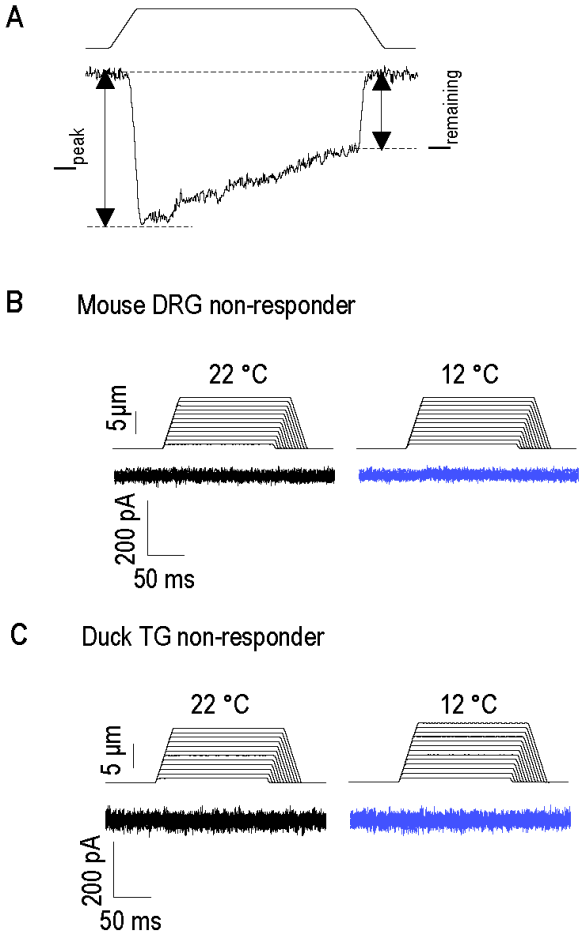

Fig. S1. Cooling does not elicit MA current from mechanically-insensitive neurons.

(A) An exemplar trace of slowly inactivating MA current in a mouse DRG neuron illustrating the measurement of fraction of remaining MA current at the end of stimulation ($I_{remaining}$) to peak (I_{peak}).

(B and **C)** Representative whole-cell MA current traces recorded from mechanically-insensitive neurons from mouse DRG (*B,* N = 5 cells) or duck TG (*C*, N = 3 cells) at 22 °C or 12 °C with indentation to the indicated depth. E_{hold} = -60 mV.

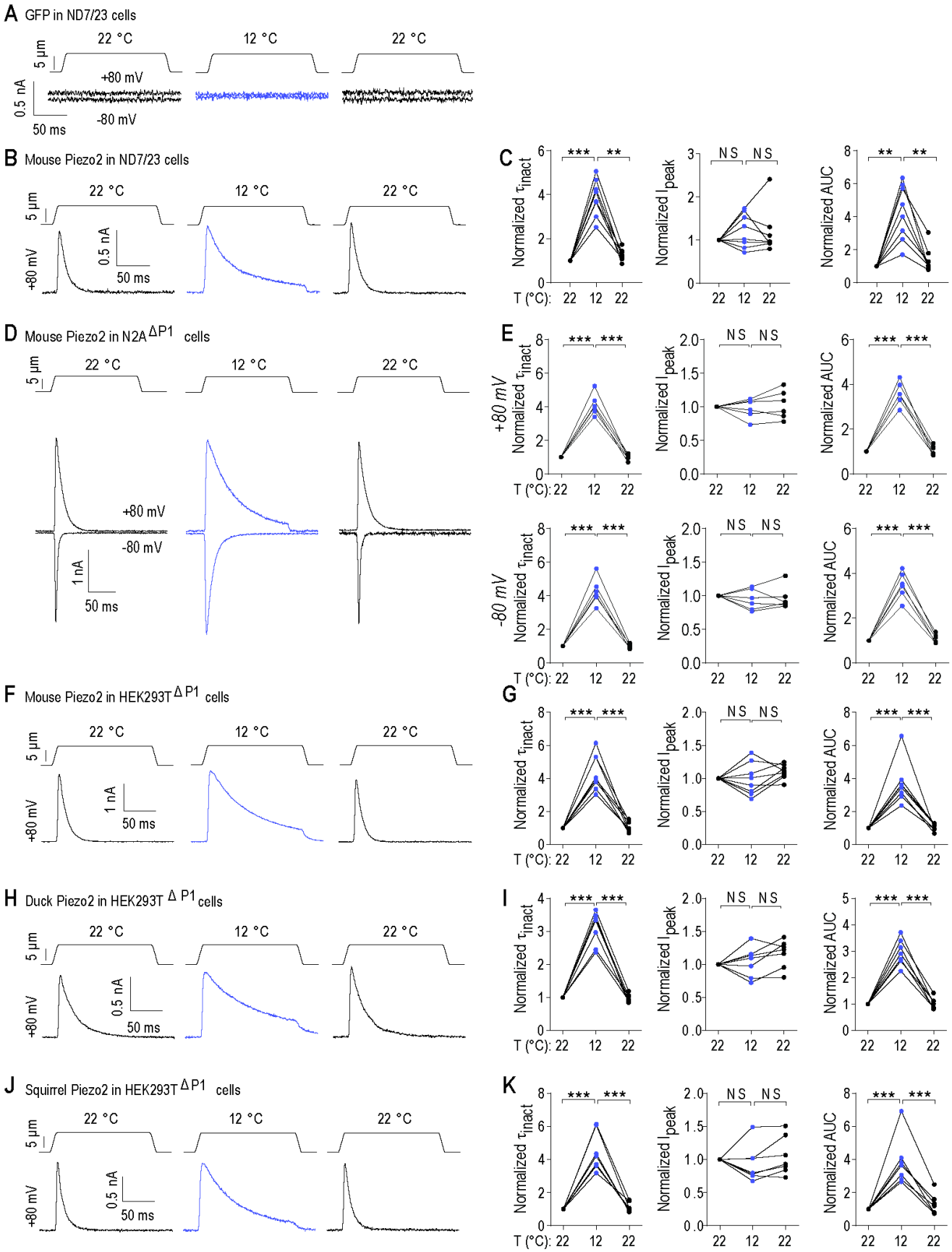

Fig. S2. Cooling potentiates Piezo2-mediated MA current.

(A) Representative whole-cell MA current traces recorded at -80 or +80 mV in the same ND7/23 cell expressing GFP (N = 7 cells).

(B and **C)** Representative whole-cell MA current traces recorded at +80 mV at indicated temperatures in the same ND7/23 cell expressing mouse Piezo2 (*B*) and quantification of normalized MA current τ_{inact}, I_{peak}, and area under current curve, AUC (*B*).

(D and **E)** Representative whole-cell MA current traces at +80 and -80 mV in the same $N2A^{\Delta P1}$ cell expressing mouse Piezo2 (*D*), and quantification of normalized MA current τ_{inact}, I_{peak}, and AUC at +80 mV (*E, upper panel*) and -80 mV (*E, lower panel*).

(F-K) Representative whole-cell MA current traces in $HEK293T^{\Delta P1}$ cells expressing either mouse Piezo2 (*F*), duck Piezo2 (*H*) or squirrel Piezo2 (*J*), and quantification of normalized MA current τ_{inact}, I_{peak}, and AUC (*G*, mPiezo2; *I*, duck Piezo2; *K*, squirrel Piezo2). E_{hold} = +80 mV.

NS, not significant, $P > 0.05$; **$P < 0.01$, ***$P < 0.001$, paired t-test.

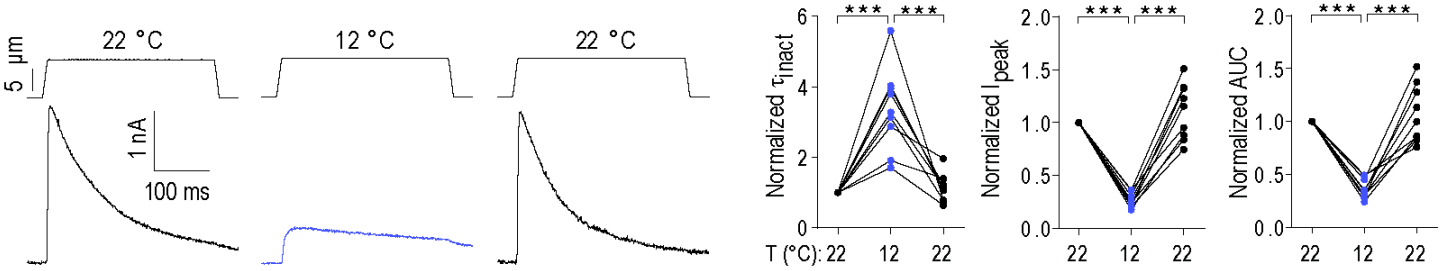

Fig. S3. Cooling inhibits Piezo1-mediated MA current.

Left panels, representative whole-cell MA current traces recorded at +80 mV and indicated temperatures in the same HEK293T$^{\Delta P1}$ cell expressing mouse Piezo1; Right panels, normalized MA current τ_{inact}, I_{peak}, and AUC. ***P < 0.001, paired t-test.

Supplementary References

1. Schneider ER, *et al.* (2017) Molecular basis of tactile specialization in the duck bill. *Proc Natl Acad Sci U S A* 114(49):13036-13041.
2. Coste B, *et al.* (2010) Piezo1 and Piezo2 are essential components of distinct mechanically activated cation channels. *Science* 330(6000):55-60.
3. Anderson EO, Schneider ER, Matson JD, Gracheva EO, & Bagriantsev SN (2018) TMEM150C/Tentonin3 Is a Regulator of Mechano-gated Ion Channels. *Cell reports* 23(3):701-708.
4. Moroni M, Servin-Vences MR, Fleischer R, Sanchez-Carranza O, & Lewin GR (2018) Voltage gating of mechanosensitive PIEZO channels. *Nature communications* 9(1):1096.
5. Dubin AE, *et al.* (2017) Endogenous Piezo1 Can Confound Mechanically Activated Channel Identification and Characterization. *Neuron* 94(2):266-270 e263.
6. Schneider ER, *et al.* (2014) Neuronal mechanism for acute mechanosensitivity in tactile-foraging waterfowl. *Proc Natl Acad Sci U S A* 111(41):14941-14946.
7. Hao J, *et al.* (2013) Piezo-electrically driven mechanical stimulation of sensory neurons. *Methods Mol Biol* 998:159-170.
8. Besch SR, Suchyna T, & Sachs F (2002) High-speed pressure clamp. *Pflugers Arch* 445(1):161-166.